Chemosphere 344 (2023) 140333

Contents lists available at ScienceDirect

Chemosphere

journal homepage: www.elsevier.com/locate/chemosphere

Pollutants abatement in aqueous solutions with geopolymer catalysts: A photo fenton case

Marina Clausi [a,1], Stefano Savino [b,1], Federico Cangialosi [c], Giacomo Eramo [a], Antonio Fornaro [d], Luca Quatraro [c], Daniela Pinto [a,**], Lucia D'Accolti [b,e,*]

[a] Earth and Geoenvironmental Sciences Department, University of Bari, Via Orabona 4, 70125, Bari, Italy
[b] Chemistry Department, University of Bari, Via Orabona 4, 70125, Bari, Italy
[c] T & A - Tecnologia e Ambiente srl, 70017, Putignano, BA, Italy
[d] Lab Service Analytica S.R.L., Via Emilia, 51/C, 40011, Anzola dell'Emilia, Italy
[e] CSGI -Center for Colloid and Surface Science Zona Osmannoro, Via della Lastruccia, 3, 50019, Zona Osmannoro, FI, Italy

HIGHLIGHTS

- Geopolymers as useful catalyst for water remediation.
- Photo-Fenton reaction as example of green oxidation.
- Heterogeneous catalysis using three dimensional approach.

GRAPHICAL ABSTRACT

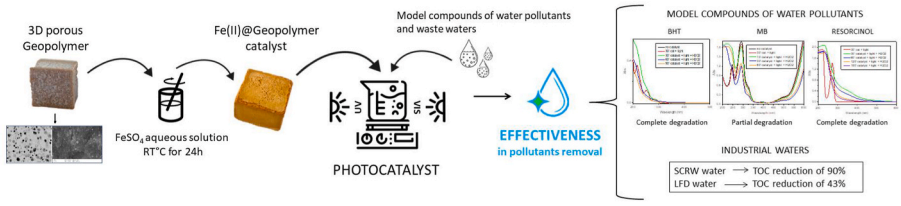

ARTICLE INFO

Handling editor: S Garcia-Segura

Keywords:
Water wastes
Geopolymers
Green oxidation
Photocatalysis

ABSTRACT

Environmental pollution is a serious threat to human health and the natural environment, and it has aroused widespread concern. One of the most effective processes in the removal of pollutants from wastewater is the Fenton reaction. This process is based on the production of highly reactive •OH radicals due to the rapid reaction between Iron ions and hydrogen peroxide under acidic conditions.

The hydroxyl radical has a high oxidation potential of $E^{\circ}(\bullet OH/H_2O) = 2.8$ V/SHE at acidic pH, so they are extremely reactive and non-selective oxidizing agent towards organic contaminants in wastewater.

In order to avoid the drawbacks of a standard Fenton reaction, a photo Fenton reaction has been tested working at neutral pH in water in the removal of refractory pollutants. For the first time, a heterogeneous system was experimented, impregnating porous metakaolin-based geopolymers, obtained by using hydrogen peroxide and vegetable oil in different ratios, as foaming agents, with iron working as photocatalyst. The dirty wastewater as scrubber water (SCRW) and liquid fraction of digestate (LFD) were tested obtaining 40–90% abatement of Total Carbon Content.

* Corresponding author. Chemistry Department, University of Bari, Via Orabona 4, 70125, Bari, Italy.
** Corresponding author. Earth and Geoenvironmental Sciences Department, University of Bari, Via Orabona 4, 70125, Bari, Italy.
E-mail addresses: daniela.pinto@uniba.it (D. Pinto), lucia.daccolti@uniba.it (L. D'Accolti).
[1] The authors Marina Clausi and Stefano Savino contributed equally.

https://doi.org/10.1016/j.chemosphere.2023.140333
Received 12 July 2023; Received in revised form 23 September 2023; Accepted 28 September 2023
Available online 7 October 2023

1. Introduction

The transition to a sustainable energy future, through the adoption of clean technologies and energy efficiency practices is fundamental for sustainable development. In particular, the wide variety of industrial processes produces a huge amount of wastewater that must be properly treated to remove chemical and biological substances and hazardous compounds, in order to be able to reuse them in the industrial cycle (Legrini et al., 1993).

Aqueous waste has always been considered as a source of organic substances to be reused to produce energy or new materials. However, in line with what has recently been highlighted by a study conducted by Unesco in United Nations World Water Development Report (www.unwater.org), the numbers concerning the water crisis reveal a dramatic scenario: about 785 million people who are denied access to drinking water; about 2 billion people without water services; about 1 million deaths per year due to lack of water, despite spending more than 260 billion dollars to combat this phenomenon. Therefore, water, like soil, cannot be considered a renewable resource and its reuse is fundamental for the harmonious development of societies.

Technological solutions are complex, requiring multiple highly articulated low energy cost processes necessary for the elimination of chemical compounds such as metals, salts, acids, bases, and volatile organic compounds (VOCs).

To this end, advanced oxidation processes (AOPs) have certainly shown potential in the treatment of various hazardous substances: chemicals such as dyes, agrochemicals, drugs, etc. More recently, advanced oxidation processes such as electrochemical oxidation (EO) treatment are being increasingly viewed as capable of providing necessary treatment (Gedam and Neti, 2014).

However, the Fenton process remains one of the most used oxidation methods in wastewater treatments due to high removal efficiency of resistant organic matter (Metin and Çifçi, 2023). Indeed, the conventional Fenton Oxidation is beneficial over other oxidation processes that can occur at room temperature and atmospheric pressure; it requires storage and inexpensive chemicals and has a high oxidation capacity. Furthermore, the process is easy to maintain and is environmentally friendly, thanks to the reduction product of H_2O_2 consisting in water (ŞefikaKaya, 2019). These processes can be conducted both through the use of hydrogen peroxide in homogeneous Fenton-type processes (Ferella, 2018) but also with molecular oxygen and metals such as copper, cerium, and other rare earths (Wang et al., 2016), using heterogeneous catalysts.

A further extension of the Fenton-like processes concerns the use of nanostructured TiO_2 or ZnO able to lead the reduction of a number of pollutants such as phenols, dyes and secondary organic pollutants such as caffeine, both through photocatalysis and photo-electrocatalysis processes (Bitenc et al., 2013; Suhadolnik et al., 2016, 2019).

The principal disadvantage of homogeneous Fenton reaction in the treatment of wastewater is represented by sludges due the precipitation of Fe(III) during the neutralization process after the oxidation reaction (Kavitha and Palanivelu, 2004). In addition, the Fenton reaction can take place at pH = 3 using H_2SO_4 which is a corrosive acid for industrial equipment.

It has been known that the mechanism of Fenton reaction involves the $OH^{\bullet}$ radical and other highly reactive activated species (eqs. (1)–(3)); beside several studies demonstrate that Fenton-type systems can be enhanced under UV light irradiation (Lofrano et al., 2009; Vorontsov, 2019; Wu et al., 1999). Indeed, the photo-Fenton reaction gives faster rates and a higher degree of mineralization than the "dark" reaction and can take advantage of light in the solar spectral region (Pignatello et al., 2006).

The mechanism reported in the following equations does not claim to be exhaustive, but reflects the fundamental steps of the Fenton and photo-Fenton processes using UV–Vis radiation and inorganic Iron salts. equations (1) and (2) show the generation of ROS radical, while eq. (3) shows the role of UV light attributed to the direct $OH^{\bullet}$ radical formation and regeneration of Fe^{+2} active species in initial chain (Vorontsov, 2019). Furthermore, the visible component of light, in the presence of dyes for example, could indirectly allow the transformation of Fe(III) in Fe(II) (eqs. (4) and (5)) (Wu et al., 1999).

Initial chain:

$$Fe^{+2} + H_2O_2 = Fe^{+3} + OH^{\bullet} + OH^{-} \quad (1)$$

$$Fe^{+3} + H_2O_2 = Fe^{+2} + OOH^{\bullet} + OH^{+} \quad (2)$$

$$Fe^{+3}(OH)^{+2} + h\nu = Fe^{+2} + OH^{\bullet} \quad (3)$$

$$\text{Substrate} + h\nu = \text{Substrate*} \text{ (visible light)} \quad (4)$$

$$\text{Substrate*} + Fe^{+3} = \text{Substrate}^{+} + Fe^{+2} \quad (5)$$

Continuing in chain transfer reaction, the hydroxyl radicals could react with organic compound forming alkyl radicals (eq. (6)) and through a series of steps allowing to produce CO_2 and water.

$$OH^{\bullet} + RH = R^{\bullet} + H_2O \quad (6)$$

Finally, the chain termination involving ROS and organic compounds giving Fe(III) and any oxidation products (Vorontsov, 2019).

Additionally, heterogeneous photo-Fenton is considered an effective method because of its characteristics of wide applicable pH range, also near the neutrality and recyclability (O'Dowd and Pillai, 2020; Vorontsov, 2019).

In any case, even the reactions in heterogeneous catalysis involve workup operations, such as filtration and/or centrifugation for the recovery of the catalyst, which involve a time and energy consumption.

To solve the problem of sludge and workup operations, a useful method is to use 3D printed catalysis (D'Accolti et al., 2023) which allows the recovery of the catalyst, simply by moving it away from the solution.

Geopolymer technology represents nowadays a promising methodology for the preparation of versatile, ease-to-design and low-impacting 3D catalysts (Hurt et al., 2017) for heterogeneous photo-Fenton processes.

Geopolymers (Davidovits, 1991) consist of three-dimensional and highly interconnected framework materials, obtained by the chemical combination of a structurally disordered aluminosilicate precursor with an alkaline activator, able to promote, at near ambient conditions, the conversion of the blend into a compact matrix (Duxson et al., 2007; Provis and Van Deventer, 2009). Geopolymers structure is mainly amorphous and consists of corner-sharing aluminate and silicate tetrahedra, with the negative charge related to AlO_4^{-} group balanced by extra-frame alkali cations (Na^{+}, K^{+} and Ca^{2+}). Geopolymers are high versatile materials, as different factors during their preparation (type of precursor and activator, curing conditions, thermal treatment, etc.) may influence their final features and properties (Shi et al., 2019). Nowadays, many studies are especially focused on the use of several kinds of industrial by-products and wastes as alternatives precursors to largely studied natural clays (i.e. kaolinitic clays) (Clausi and Pinto, 2023; D'Elia et al., 2023; Khalifa et al., 2020). However, since the chemical composition and mineral phases usually vary in different raw materials, the properties of geopolymers produced can significantly differ between each other. Hence, pure kaolinitic clays (Duxson et al., 2005) is the most suitable precursor for high standards materials and technical applications.

The number of studies concerning geopolymers or alkali activated materials (other name by which these materials are known) increased significantly in the recent years (Gökçe et al., 2021), as they are environmental-friendly due to a low temperature production process, are highly versatile and may show high durability and mechanical resistance (Bernal and Provis, 2014; Zhang et al., 2017). Many studies were addressed to construction industry, evaluating the performance of geopolymers as alternative binders to traditional ones (Shehata et al.,

2021), but recently, new research have been geared into their utilization for nontraditional applications such as in water and wastewater treatment (adsorbents/ion-exchangers, membranes and filtration media, water stabilization and pH regulators and wastewater treatment residues) (Ettahiri et al., 2023; Li et al., 2022; Luhar et al., 2021; Luukkonen et al., 2019; Medri et al., 2022; Vitola et al., 2020). It is worth noting that, for these emerging applications, several methods for controlling porosity through the use of additives or specific manufacturing processes to modify the conventional geopolymer structures, are often experimented (Novais et al., 2020).

Among the emerging applications, promising results were obtained by experimenting geopolymers as catalysts. In a recent review by Zhang and co-authors four categories of geopolymer catalysts were identified: geopolymers served as catalysts directly, ion-exchange geopolymer catalysts, loaded geopolymer catalysts, and carbon improved geopolymer catalysts ((Zhang et al., 2020) and references therein). Some studies explored the use of geopolymers as photocatalysts in "end-of--pipe" treatments, mainly for degradation of dyes from wastewater (El Alouani et al., 2019; Falah et al., 2016; Zhang et al., 2013). More recently, other studies concerned the degradation activity of biochar/geopolymer composites (Huang et al., 2023; Zhu et al., 2022) and pollutans oxidation by using Co(II)-coated geopolymer foams (Luukkonen and von Gunten, 2022) and NiO/geopolymer nanocomposites (Abukhadra et al., 2022). Instead, no application of geopolymers in heterogeneous photo-Fenton catalysis for the wastewater treatment is known in literature.

In the light of these considerations, in this paper Fe(II) impregnated geopolymer composite materials were prepared to develop an environmentally sustainable method for the recovery of industrial water. The catalysts were characterized with a multianalytical approach consisting of X-ray diffraction, XPS and FT-IR spectroscopy, optical and electron-scanning microscopy were applied to the three compounds Methylene Blu, Benzothiazole, and Resorcinol used as model of water pollutants. Our method was then applied efficiently to two types of dirty water, such as the scrubber water and liquid fraction of digestate, with the final aim of reusing the clean water for industrial application with a circular economy approach (see Supplemental materials for the list of abbreviation).

2. Materials and methods

Materials and Characterization methods were reported in detail in Supplemental Material.

Samples label	GP_1HO	GP_5HO	GP_10HO	GP_1HO_20O	GP_5HO_20O	GP_10HO_20O
Foaming agents [wt%]	H_2O_2 = 1%	H_2O_2 = 5%	H_2O_2 = 10%	H_2O_2 = 1% + Olive oil = 20%	H_2O_2 = 1% + Olive oil = 20%	H_2O_2 = 1% + Olive oil = 20%
Bulk density [g/cm³][a]	1.50 (0.20) [b]	1.30 (0.05)	1.02 (0.04)	2.33 (0.02)	1.19 (0.07)	0.93 (0.02)
Integrity test [24h]	No cracks	No cracks	No cracks	No cracks	No cracks	No cracks
Stability test [10 days]	No cracks	No cracks	No cracks	No cracks	Slight fragmentation	Slight fragmentation
Porosity [%][c]	33.6	44.9	57.1	9.8	66.7	73.6
Represent-ativeness	0.010	0.040	0.089	0.003	0.004	0.039
mean size large pores [mm] [c]	0.200 (0.100)	1.243 (0.500)	1.651 (0.764)	0.234 (0.114)	0.224 (0.082)	0.652 (0.296)
mean size small pores [mm] [c]	//	//	//	0.011 (0.007)	0.011 (0.008)	0.013 (0.007)
Macro images						
OM [8x]	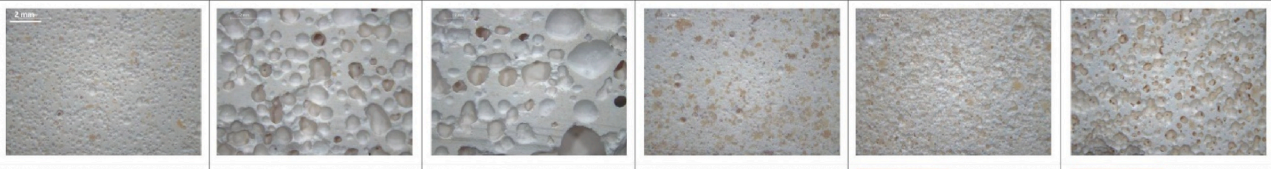					
SEM [80x][d]	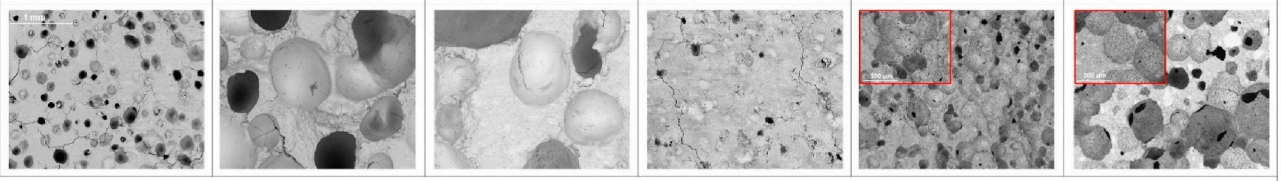					

[a] Calculated from the ratio between the mass (g) and the geometrical volume (cm^3) measured with a calliper on monoliths. [b] Standard deviation in round parenthesis. [c] Pore percentage and size determined by IA. [d] The insets of GP_5HO_20O and GP_10HO_20O show the magnified view (200x) of a group of cells. Scale bars are reported in GP_1HO column.

Fig. 1. Details of porous geopolymers. Each column refers to one sample; sample names are reported on the top of the columns.

2.1. Catalyst preparation

2.1.1. Synthesis of geopolymers

Porous geopolymers were obtained by blending kaolinite clay heat-treated at 700 °C for 2 h (MkB) and a sodium silicate solution, modified by adding distilled water and sodium hydroxide, in order to obtain samples characterized by the following molar ratios: $SiO_2/Al_2O_3 = 3.6$, $Na_2O/SiO_2 = 0.3$, $H_2O/Na_2O = 12$, $Al_2O_3/Na_2O = 1$. Mixing operations were performed for 10 min at 1200 rpm. To promote porosity, hydrogen peroxide H_2O_2 (3 wt% diluited) in different weight ratios (1–5–10%) and/or olive oil in weight ratio 20% were added, based on findings by Bai et al. (2016); Bai et al. (2016), who showed out that olive oil provides a better combination in terms of porosity and mechanical strength than other vegetable oils. Slurries were stirred for 5 min at 600 rpm or 10 min at 1200 rpm, respectively. Blends were poured into cubic steel moulds (20 × 20 × 20 mm^3), compacted by mechanical vibration to remove air and cured in three steps: overnight at room temperature, then at 85 °C and 100% R.H for 8 h and three days sealed at room temperature. A set of six different geopolymer samples was prepared for the subsequent test (Fig. 1).

The integrity of samples after immersion in distilled water (weigh ratio sample/water 1:10) at room temperature for 24 h was evaluated according to the test described in Lancellotti et al. (2013). Samples were soaked in water for further 10 days to evaluate their structural stability in water. During this span of time, water was regularly changed and pH measurement was performed each 8 and 24 h, until pH of immersing water reached constant values.

Before the preparation of the catalysts, one samples of each series was subjected to washing in distilled water to eliminate the excess of soluble ions. Anyway, more cycles of washing were necessary for the samples containing olive oil (until water remained clear) to reduce soluble molecules generated by the saponification (Bai et al., 2016).

2.1.2. Preparation of the catalytic system

The prepared cubic geopolymer monoliths (2 × 2x2 cm) were used as a support for the Fe-based catalyst. In order to create the catalytic system a Fe(II) sulphate aqueous solution ($[FeSO_4] = 0.2$ M, 2.78 g, 10 mmol in 50 mL of distilled water, pH 3.48) was prepared and the geopolymer was impregnated at room temperature under stirring for 24 h (pH 4.68, mass ratio of water and geopolymer W/GP = 25). Impregnation was performed both on as-prepared geopolymer samples and in samples previously washed, as described above.

2.1.3. Photo Fenton process

In order to validate the efficiency of the catalytic system, different model molecules of aqueous pollutant were tested: benzothiazole (BTH), resorcinol, and methylene blue (MB). For this reason, aqueous solutions were prepared with the following concentrations: benzothiazole = 0.74 × 10^{-4} M resorcinol = 0.01 M and methylene blue = 0.001 M. The photoreactor used is equipped with a jacket for the circulation of cooling water and with two lamps: HRC UV–Vis 300 W (Sanolux) lamp and Xe-Halogen 400 W (Radium) lamp, both placed at 13 cm from the reactor (see supplemental materials for the spectra). A known volume (50 mL) of aqueous pollutant solution was transferred in the reactor with the functionalized geopolymer under stirring. The cooling system was activated, and the lamps were turned on. After 30 min, from 0.2 to 1 mL of hydrogen peroxide 9.8 M (3.9 × 10^{-2} M–0.19 M respectively) was added and every 30' analysis was carried. The degradation of the pollutants was monitored using an UV–Vis spectrophotometer and monitoring the maximum of absorption.

2.1.4. Geopolymers regeneration

For the regeneration of the catalyst, an aqueous solution of hydroxylamine hydrochloride (7,8 × 10^{-2} M, 0.27 g 3.9 mmol in 50 mL) was used, in ratio water and geopolymers W/GP = 25. The geopolymer was soaked in the solution of hydroxylamine hydrochloride for 30' under stirring.

2.1.5. Photo Fenton treatment of wastewaters

Organic waste treatment plants (aerobic or anaerobic) produce wastewater with a very high TOC content. The exhaust air of an aerobic composting plant is constantly scrubbed in the column during wet scrubbing treatment, while the aqueous phase is circulated in countercurrent mode: the scrubbing water (SCRW) absorbs and/or chemically reacts with the organic contaminants and must be treated for TOC reduction in order to be reused in the process. In anaerobic digestion plants, on the other hand, liquid fraction of digestate (LFD) is the wastewater deriving from the raw digestate dewatering stage, and is characterized by a very high ammonia and TOC content. Samples of scrubbing water (SCRW) and liquid fraction of digestate (LFD) were tested.

50 mL of wastewaters were transferred in the reactor with the functionalized geopolymer under stirring. The cooling system was activated, and the lamps were turned on. After 30 min, from 5 mL of hydrogen peroxide 9.8 M was added and the reaction with TOC analysis after the quenching with appropriate amount of sodium thiosulfate.

3. Results and discussion

To verify the potential of geopolymer catalysts in photo Fenton processes, preliminarily benzothiazole (BHT), as a model molecule for secondary pollutants (antibiotics, drugs, etc.) (Reynoso et al., 2021), then methylene blue (MB), which can be considered as a model compound for many degradation studies (Antonopoulou et al., 2014; Wang et al., 2016), and resorcinol, as a model for phenols pollutants (D'Accolti et al., 2023), were tested. Finally, industrial waters such as scrubbers and urban landfill waters were studied as real water.

3.1. Geopolymer characterization

Kaolinite clay (KaoB) used as raw material for the preparation of the geopolymer catalyst is characterized by high silica and alumina content (SiO_2+Al_2O_3 = 85.81 wt%), low alkali percentages and crystalline phases consisting of kaolinite (~88 wt%), quartz (~6 wt%), with minor illite/muscovite (~2.5 wt%) and K-feldspar (~3 wt%) (Table 1s, Supplemental materials).

XRPD, FTIR and SEM techniques were used to assess the geopolymerization reaction from the comparison of geopolymer samples with metakaolin (MkB) used as precursor (kaolinite clay heated to 700 °C). All the analyzed samples showed similar features, so only results related to GP_1HO are discussed hereafter. XRPD pattern of GP_1HO (Fig. 2s, Supplemental materials) shows the formation of the typical hump in the 20–35° 2θ range, related to the amorphous phase which characterizes geopolymers; quartz and traces of illite/muscovite

Table 1
Photo-Fenton experimental.[a].

entry	wastewater	Time (minute)	TC mg/L	TOC[b] mg/L	IC mg/L	% of abatment
1	SCRW	0	13190	12270	920	——
2	SCRW	15	5497	4908	589	40
3	SCRW	30	1196.2	1177	18.8	90
4	LFD	0	6060	3926	2135	——
5	LFD	15	2833	2800	28	29
6	LFD	30	2985	2900	74	28
7	LFD	60	2390	2250	136	43

[a] In 50 mL of wastewater was added 5 mL of H_2O_2 (9.8 M).
[b] The reaction was monitored with the amount of 10 mL the solution using quenchers 0.3–0.6 g of $Na_2S_2O_3$ as quencher before determining the TOC, to avoid over oxidation.

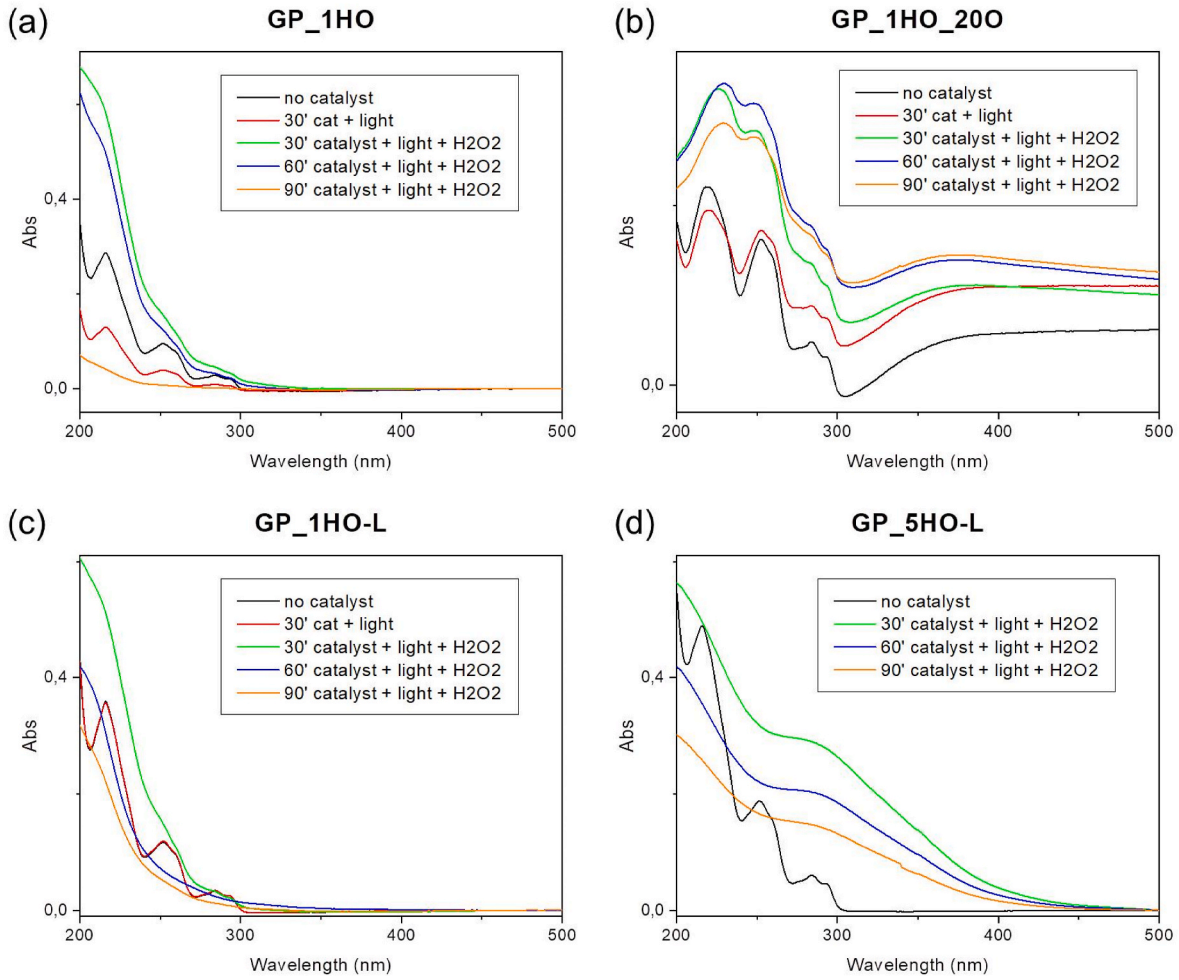

Fig. 2. UV–Vis spectra of experiments carried out using unwashed GP_1HO (a) and GP_1HO_20O (b) at pH 10 and washed GP_1HO-L (c) and GP_5HO-L (d) at pH 7.8.

are present as unreacted crystalline phases.

FTIR spectrum of GP_1HO (Fig. 2s, Supplemental materials) shows a main band, centred at 1028 cm^{-1}, shifted to lower wavenumbers compared to MkB one. This band is considered the fingerprint of aluminosilicates (Si–O-T bonds, in which T is Al or Si in tetrahedral coordination) and the observed shifts accounts for the geopolymerization reaction (Lee and Van Deventer, 2003). The broad band at 3440 cm^{-1} and the peak at 1645 cm^{-1} is related to O–H stretching and bending modes of molecular water, respectively; however, the presence of water should be also ascribed to its absorption onto the surface. Other bands detected are at 880 cm^{-1} related to Si–O and Si–OH vibrations and the peaks at around 450 and 780 cm^{-1} associated to Si–O–Si vibrations of quartz.

SEM analyses show dense and well-developed amorphous matrix formed only by compacted globular units, further confirming the completeness of the geopolymerization reaction (Fig. 2s(c), Supplemental materials).

Integrity tests in distilled water gave successful results for all the samples: undamaged surfaces without any cracks were noted independently of the physical characteristics of samples (Fig. 1). This test allows to obtain direct feedback on the completion of the geopolymerization reaction, as water leads to disaggregate geopolymer structure if the process is non-fully occurred (Cilla et al., 2014; Sgarlata et al., 2022). Keeping samples in water for further 10 days confirmed their structural stability. Some isolated fragments were noted only in the water containing GP_5HO_20O and GP_10HO_20O at the end of the experiment. At the beginning of the test, waters showed basic pH values (about 12) due to Na^+ ions release from the samples. After 10 days, pH values decreased to about 8 for all samples, with slightly higher values measured on waters containing GP_5HO_20O and GP_10HO_20O samples.

The bulk density of samples varies from 2.3 to 0.9 gr/cm^3 showing a trend decreasing with the amount of H_2O_2 used in the sample preparation.

The comparison of macroscopic and microscopic images of different porous geopolymer samples (Fig. 1) shows out how the different concentration of hydrogen peroxide and the addition of olive oil in the mix, affected the percentage of porosity and the pore size distribution. While the use of H_2O_2 alone, gives rise to mainly closed cells with unimodal pore size distribution and mean shifting toward higher values with increasing the H_2O_2 concentration, the combination of H_2O_2 and olive oil allows the development of an interconnected porosity and a further population of micropores of about 100 μm in diameter, resulting in a bimodal size distribution of pores (Table 1). Among oil-free test specimen, circular shaped macro-pores with regular borders (0.2 mm mean size) can be distinguished in GP_1HO, whereas GP_5HO and GP_10HO are characterized by sub-spherical (1.243 mm mean size) and irregular or sub-rounded (1.651 mm mean size) shaped cells, respectively. It is worth noting that the population mean and the standard deviation of the small pores is quite similar for the samples mixed with olive oil, whereas a largest variability was observed in the macro pores of oil-free samples. Moreover, the addition of olive oil to the mix seems to regulate the formation of macro pores too. According to Bai et al. (2016) the features of oil-prepared samples are due to holes produced by oil droplets trapped in the geopolymer structure and removed by the water washing. The addition of oil promotes both the formation of a foam (surfactant molecules) and a change in slurry viscosity which contributes to contain,

more or less significantly, the oxygen bubbles generated by the peroxide decomposition (Bai and Colombo, 2018; Medpelli et al., 2014). The results agree with previous studies concerning the influence of foaming agents on the geopolymer features (Bai et al., 2016, 2017; Cilla et al., 2014; Papa et al., 2022).

3.2. Screening tests of geopolymers catalysts and recycle

Preliminary to all experiments with geopolymers, we tested kaolin powder as a background reaction, which showed no reactivity, than the geopolymers were used for the preparation of the catalyst for photo Fenton reaction by impregnation with an aqueous solution of Fe(II) sulphate following the procedure described in experimental section and using two different light source (HRC UV–Vis 300 W lamp and Xe226 Halogen 400 W lamp) to cover all UV–vis spectra (Fig. 3s, Supplemental materials).

To obtain the best three-dimensional support, we decided to test both the geopolymer prepared with oil and without oil, both as it is and washed with distilled water several times to eliminate the excess of soluble ions and to reduce, in the case of oil-bearing samples, the soluble molecules generated by the saponification (the washed samples are labelled with the letter L at the end of the name).

Although the impregnation procedure was maintained the same for all the samples, the final result is slightly different for the samples impregnated. Indeed, for the unwashed geopolymer GP_1HO and GP_1HO_20O can be seen that the impregnated geopolymer presents inhomogeneous spots where there is a major concentration of deposited Iron or on the contrary a lack of it. Hypothetically, this can be caused by the unwashed sample changing the pH of the solution. On the other hand, the washed GP_1HO-L and GP_1HO_20O-L show a homogeneous distribution of the Fe(II) sulphate solution, also confirmed by the SEM analysis (see Fig. 5, Table 2s in Supplemental materials).

Preliminary, we decided to test all the catalysts using the benzothiazole as model compound (Bahnmüller et al., 2015), with reaction conditions reported in experimental section, using 50 mL of water solution (3.7×10^{-3} mmol) and excess of H_2O_2 (0.2 mL 1.96 mmol, 3.9×10^{-2} M) (D'Accolti et al., 2023; Reynoso et al., 2021). The BTH degradation by photo-Fenton processes was measured at different reaction times, using the UV–Vis spectrophotometer and monitoring the decay of the maximum of absorption around 217, 252, 294 nm.

Moreover we verified that both $FeSO_4$ and H_2O_2 didn't interfere with the maximum of absorption of the pollutants (see Fig. 4s of Supplemental materials for the registered UV–Vis spectra).

We started our experiment using unwashed catalysts: GP_1HO (Fig. 2a) and GP_1HO_20O (Fig. 2b) (see abbreviation in Supplemental materials) working at pH 10 due to the fact that both geopolymers had not been washed following their preparation. The UV–Vis spectra reported in both Fig. 2a and b shows that after 30 min of irradiation of solution (red line), the absorbance decreases, while the UV–Vis spectrum profile of the BHT does not change, suggesting that there were no auto-photolysis processes. The decreases of the absorbance could be due to adsorption phenomena owing to the low solubility of BTH in water (Bahnmüller et al., 2015). Then, after the addition of H_2O_2 in 90 min the GP_1HO_20O catalyst did not show any degradation (Fig. 2b), conversely the GP_1HO catalyst showed a good efficiency after 30 min (Fig. 2a, green line), in fact the signal at 217 nm disappeared and finally at 90 min the degradation was complete. Considering these results, no further test was performed on samples prepared adding olive oil, whereas we decided to test the GP_1HO-L, to verify the effect of the pH.

Indeed, the washed catalyst allowed working at a pH close to neutrality, resulting in a pH = 7.8 of BHT solution after immersion of the catalyst. As reported in Fig. 2c, in this case the degradation occurred without preliminary adsorption (black and red line overlap) and showed the complete change of the UV–Vis spectrum (green line) after 30 min, while after 90 min (orange line) the degradation was complete. This result is comparable to the same reaction conducted using homogeneous catalysis (Reynoso et al., 2021).

To verify the effect of increasing the porosity of the geopolymers, the sample GP_5HO-L (prepared with 5 wt% of H_2O_2) was tested (Fig. 2d). Although the reaction took place, the catalyst partially flaked off during the reaction. For this reason, no further tests were performed on the sample GP_5HO-L.

The absence of leaching of Iron into the reaction mixture was ascertained by the hot filtration test after 60 min of the reaction, thus stopping the reaction.

Based on the overall discussed experiments, GP_1HO-L has been selected as the most suitable catalyst for subsequent tests, as it allows avoiding adsorption effects and the flake off of the material, as well as leaching of active catalytic species.

Finally, in a control experiment, the reaction was also carried out in dark conditions and as expected the degradation did not complete as shown in Fig. 3a (purple line) and in the insert where the signal at 252 nm is still present.

This latter result is in accordance with XPS analysis of GP_1HO-L impregnated with Fe(II)SO_4. In particular, the high-resolution XPS Fe $2p_{3/2}$ signal in Figs. 5s and 6s (supplemental material) presents a peak component at about 710.5 eV ascribed to Fe(II)O together its corresponding shake-up satellite peak at 716.2 eV. The component at 712.5 eV could be due to both $FeSO_4$ and Fe(III) oxide as reported in the literature (Grosvenor et al., 2004; Mills and Sullivan, 1983; Wang and Zhang, 2023). The presence of Fe(III) oxide is also confirmed by the Fe (III) shake-up satellite peak at 719.5 eV (Grosvenor et al., 2004; Mills and Sullivan, 1983; Wang and Zhang, 2023).

To verify the recyclability of the catalyst, the reaction was carried out for three times, regenerating the catalyst with hydroxylamine hydrochloride, as reported in the literature (D'Accolti et al., 2023; Zheng et al., 2022). In particular, the catalyst was immersed in a hydroxylamine hydrochloride aqueous solution (7.8×10^{-2} M) for about 30 min,

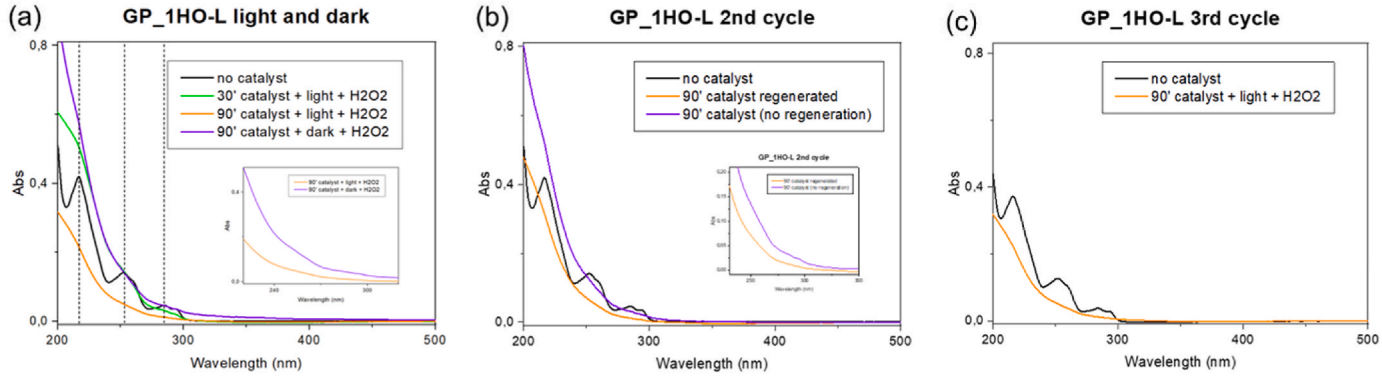

Fig. 3. UV–Vis spectra of BHT in recycles experiments.

Table 2
Comparison of the efficiency of GP_1HO-L catalyst with the literature data.

Entry	Catalysts	Substrate	Time minute	Temperature °C	Conv. %	Ref
1	Homogeneous Photo Fenton	BHT	60	25	80	Reynoso et al. (2021)
2	Fe(II)-3D-printed PLA	BHT	200	25	100	D'Accolti et al. (2023)
3	GP_1HO-L	BHT	90	25	100	Our work
4	Heterogenous -Fe2O3@GO	MB	40	25	100	Liu et al. (2017)
5	Fe(II)-3D-printed PLA	MB	40	25	100	D'Accolti et al. (2023)
6	GP_1HO-L	MB	60	25	40	Our work
7	Photo-fenton	resorcinol	240	25	85	Barona et al. (2015)
8	Fe(II)-3D-printed PLA	resorcinol	120	25	100	D'Accolti et al. (2023)
9	GP_1HO-L	resorcinol	120	25	100	Our work

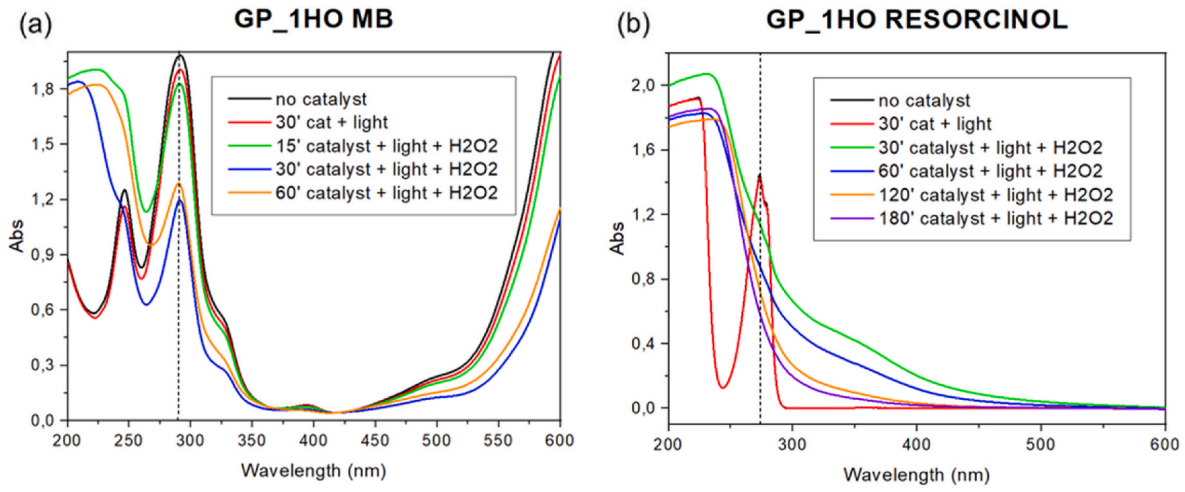

Fig. 4. UV–Vis spectra for the photofenton reactions for Methylene Blue (a) and Resorcinol (b). (For interpretation of the references to color in this figure legend, the reader is referred to the Web version of this article.)

and briefly dried, then being ready. The XPS analysis after this treatment (Fig. 7s in supplemental materials) shows that the composition of Fe in the catalyst is very similar, which further confirms that the prepared catalyst is robust and can be easily recycled.

In both case the presence of Fe(II)SO_4 were confirmed from the EDS analysis reported in Table 3s (supplemental material), that showed the presence of Sulphur correlating very well with Iron content.

Fig. 3 shows that the BHT degradation takes place in three consecutive experiments carried out using the same catalyst after regeneration with hydroxylamine hydrochloride.

In addition, in this case we carried out a control experiment by recycling the sample without pre-treatment and as shown in Fig. 3b there is still a residual of the signal both around 252 and 294 nm after 90' using the catalyst without the regeneration step. This shows that the reaction is less efficient because the Fe(III) must be preliminarily photo reduced into Fe(II) as shown by equations (3)–(5) (Pignatello et al., 2006; Kavitha and Palanivelu, 2004; Vorontsov, 2019).

Therefore, we can conclude that during the Fenton reaction there is no relevant Fe(II/III) leaching affecting the catalytic activity in three consecutive cycles of reactions and regenerations. In fact, as reported below (3.4 section), the composition of the catalyst after the first cycle GP_1HO-L_R1 seems quite similar to GP_1HO-L_R0.

Conversely, GP_1HO-L is no longer reusable for a fourth cycle as it partially flake off, as also attested by SEM analysis of the catalyst after the reactions (see paragraph 3.4).

3.3. Screening of pollutants

The extensive application of dyes, flavour compounds (often derived from phenol), and BTH in industrial and consumer products has led to widespread contamination of the environment. Various methods have been adopted for the degradation of these pollutants (Antonopoulou et al., 2014; Reynoso et al., 2021), but, in most cases, oxidative processes based on H_2O_2 and UV–Vis are used, which are not industrially viable. The geopolymer technique seems suitable for this application and in particular, the GP_1HO-L appears to have the best performance therefore it has been chosen for the degradation of MB and resorcinol.

Fig. 4a highlights that photo-Fenton reaction, although capable of oxidizing the MB using H_2O_2 in excess (0.5 mL of H_2O_2, 9.7×10^{-2} M), in reality fails to degrade it completely, which is due to the scattering of the solution which is particularly dark. In any case, after 60 min (orange line) it is possible to see a reduction in absorbance of 40%, in the region of 291 nm. This latter value is quite different compared to the literature using the heterogenous Fe_2O_3@GO, that is more efficient, but also expensive (Liu et al., 2017).

Conversely, the resorcinol reacts with H_2O_2 (1 mL, 19×10^{-2} M) after 30 min (green line with the disappearance of the signal at 280 nm (Fig. 4b). This result is comparable with an analogous reaction on the catechol always conducted under conditions of homogeneous photocatalysis (Charcosset, 2009).

3.4. 4. Characterization of catalysts after reaction

SEM-EDS investigations were performed to investigate the microstructure of the geopolymer catalysts after photo-Fenton experiments to assess possible changes or degradation effects. In Fig. 5 SEM-BSE images and X-ray elemental maps of catalyst surfaces after one and three regeneration cycles (GP_1HO-L_R1 and GP_1HO-L_R3, respectively) are reported in comparison with the fresh geopolymer sample (GP_1HO) and the Fe-based catalytic system before photo-Fenton experiments

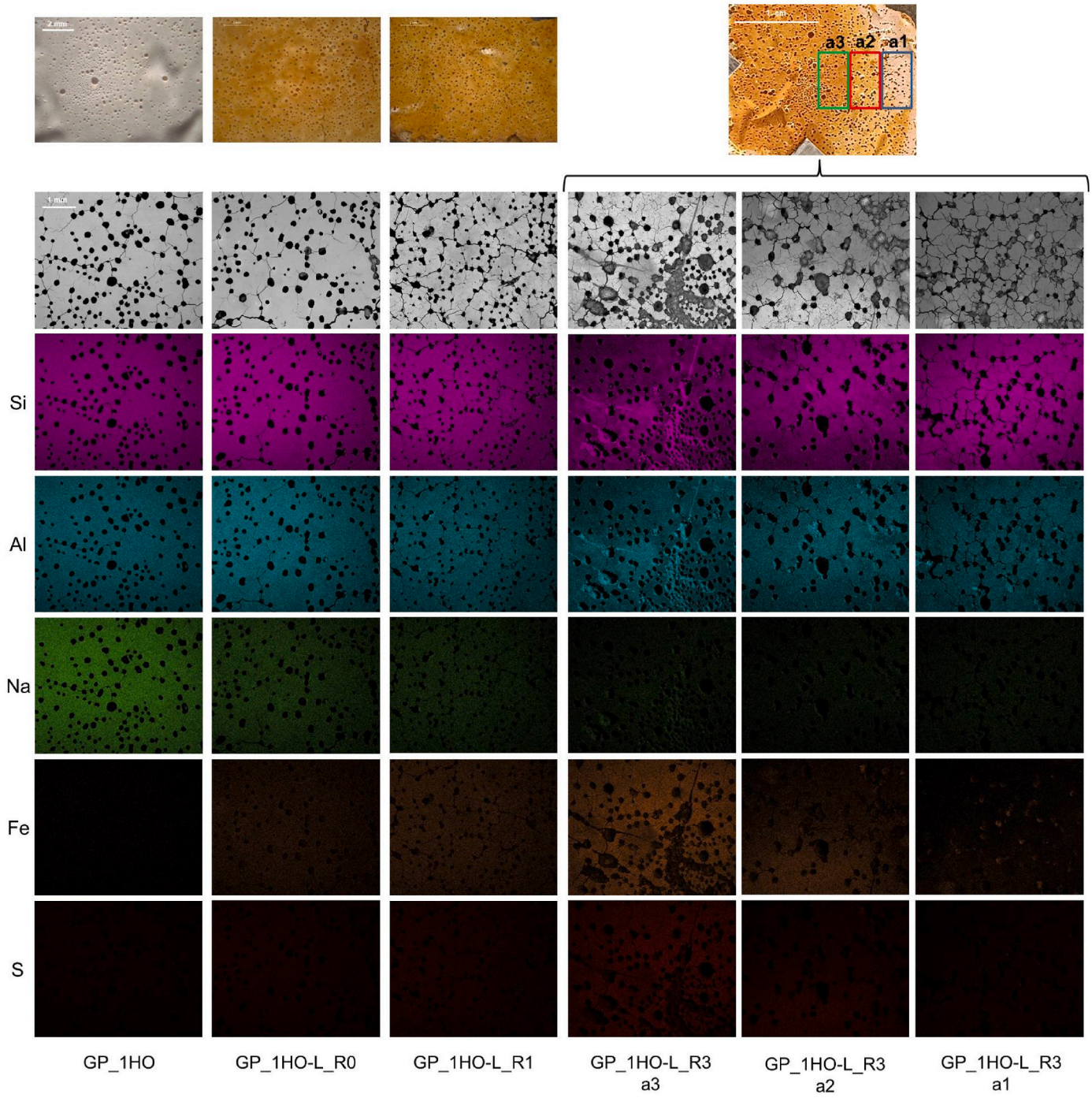

Fig. 5. SEM-BSE images (enlargement 50x) and SEM-EDS elemental maps of catalysts. Each row refers to one chemical element; each column refers to one sample or to the analysis of a portion of it. Samples name are reported on the bottom of each column. GP_1HO is reported as reference; suffixes RO – R1 – R3 indicates the numbers of regeneration cycles of GP_1HO-L sample. Macroscopic or stereomicroscopic (enlargement 8x) references are also reported.

(GP_1HO-L_R0). Images by optical microscopy of the same samples are shown on the top of Fig. 5, as well. From both OM and Fe-map images the uniform distribution of the Iron on the geopolymer matrix can be appreciated, attesting the high efficiency of the impregnation treatment (sample GP_1HO-L_R0). EDS analyses on the surface of the geopolymer show an average Fe content of 9.7 wt% (± 1.6). The sample GP_1HO-L_R1 regenerated only one time, shows surface elemental distribution similar to GP_1HO-L_R0, with the exception of a slight increase of Fe (around 14.8 ± 1.6 wt%) and decrease of Al, but appears slightly more fractured. Furthermore, both the samples GP_1HO-L_R0 and GP_1HO-L_R1 show a significant decrease of sodium, which halves with respect to the fresh geopolymer, probably due to the pre-washing of the samples before the tests. After three regeneration cycles the geopolymer catalyst (sample GP_1HO-L_R3) shows more fractured and non-homogeneous surfaces, consisting of portions with a different relative distribution of the Fe-sulphate embedded to the porous geopolymer matrix. EDS analysis showed out concentration of Fe ranging from 2.8 wt% up to 30.6 wt % on the geopolymer surface. This evidence, associated to a slight proportional increase of Si/Al ratio in Fe-poorest portions of GP_1HO-L_R3 (from 2.14 on fresh GP_1HO to lower than 4.16 wt%) and to a significant loss of Na on the whole surface of this sample (from about 10 wt% on fresh geopolymer GP_1HO to lower than 1 wt%), suggests a

slight degradation at the surface of the geopolymer catalyst after the three reaction/regeneration cycles (see also Table 3s in supplemental materials).

3.5. Test on real wastewater samples from organic waste treatment plants

As already mentioned, water is used to realize various types of essential needs such as drinking, irrigation, cleaning, construction, industrial operations, and in each phase of life and nutrient cycle. Out of the total water present, 0.3% of water is useful to human race and other 99.7% is no useful water. This small portion of water is directly accountable for the sustainability of living organisms on Earth, and therefore it needs to be protected from pollution, for this reason, it is necessary both to protect this resource, but also to try to recycle industrial waters. In this work we have decided to apply the method we have developed, which makes use of geopolymers as supports for the heterogeneous catalysis in the photo-Fenton reaction, to two industrial waters, which are normally considered waste: scrubbing water (SCRW), and liquid fraction of digestate (LFD). The first one, with pH 4.8, has total carbon oxidable (TOC) of 12270 mg/L (Table 1, entry 1). The deep brown effluent LFD with pH 6.8 contained TOC in the range 3926 mg/L (Table 1, entry 4) and 7451 Cl^- mg/L and 6860 ppm of NH_4^+.

In the light of this analysis, it is evident that the Photo Fenton method is the most suitable for the abatement of pollutants in water because it also allows to work at acid pH < 7 and is not affected by the presence of chlorides (Reynoso et al., 2021), conversely to the Fenton process (Lu et al., 2005). The data reported in Table 1 showed that the photocatalytic process is particularly effective in the case of SCRW waters as after only 30 min the TOC reduction is 90% (Table 1, entry 3). In the case of LFD water, the reaction is less efficient: after 15 min the reduction is 29% (Table 1, entry 5) and only after 60 min the reaction allows for a reduction of 43% (Table 1, entry 6).

A possible explanation for the lower efficiency of the photocatalysis process for LFD waters is the scattering of light due to the deep brown color.

In any case, this result is competitive when compared with much more complex processes, such as continuous electrolysis in carbon bed (Gedam and Neti, 2014).

4. Conclusion

In conclusion, continuing our effort in green catalysis (Fusco et al., 2022; Pantone et al., 2017) and innovative materials, the use of geopolymer catalysts opens the way to new catalytic applications, especially in the environmental field.

Indeed, the photo Fenton process presented in this work does not lose efficiency compared to those reported in the literature (see Table 2).

Moreover, it does not generate sludge to be disposed of and the workup of the reaction is particularly simple. Furthermore, the study conducted on real industrial waters shows how it can also be applied in complex mixtures, which represents an advance compared to current AOP catalysis studies.

In addition, our method resolves the problem of the sludge normally obtained using the traditional homogeneous and heterogenous reaction, reducing the wastes in according of the rule of green chemistry.

With this in mind, different developments can be thought for future application of geopolymer catalysts as wastewater treatment agents for industrial purposes. In this perspective, further tests on real matrixes and a better optimization of the catalysts will be needed, but these starting tests were really encouraging.

CRediT authorship contribution statement

Marina Clausi: Investigation, Writing – original draft. **Stefano Savino:** Investigation, Writing – original draft. **Federico Cangialosi:** Data curation. **Giacomo Eramo:** Investigation. **Antonio Fornaro:** Data curation. **Luca Quatraro:** Investigation. **Daniela Pinto:** Conceptualization, Methodology, Writing – original draft. **Lucia D'Accolti:** Conceptualization, Methodology, Writing – original draft.

Declaration of competing interest

The authors declare the following financial interests/personal relationships which may be considered as potential competing interests: Lucia D'Accolti, Daniela Pinto, Antonio Fornaro, Federico Cangialosi reports financial support was provided by Ministry of the Environment and Energy Safety.

Data availability

all the data is in the paper

Acknowledgement

This work was funded by the MASE (Ministero dell'Ambiente e della Sicurezza Energetica, ITALY) Project WASP grant number H93C22000360004. Thanks are due at Dr. Fiorenza Fanelli (research CNR-Italy, Nanotec) for XPS analysis and helpful discussion.

Appendix A. Supplementary data

Supplementary data to this article can be found online at https://doi.org/10.1016/j.chemosphere.2023.140333.

References

Abukhadra, M.R., AlHammadi, A.A., Khim, J.S., Ajarem, J.S., Allam, A.A., Shaban, M.S., 2022. Enhanced adsorption and visible light photocatalytic removal of 5-Fluorouracil residuals using environmental NiO/geopolymer nanocomposite: steric, energetic, and oxidation studies. J. Environ. Chem. Eng. 10, 108569 https://doi.org/10.1016/j.jece.2022.108569.

Antonopoulou, M., Evgenidou, E., Lambropoulou, D., Konstantinou, I., 2014. A review on advanced oxidation processes for the removal of taste and odor compounds from aqueous media. Water Res. 53, 215–234. https://doi.org/10.1016/j.watres.2014.01.028.

Bahnmüller, S., Loi, C.H., Linge, K.L., Gunten, U. von, Canonica, S., 2015. Degradation rates of benzotriazoles and benzothiazoles under UV-C irradiation and the advanced oxidation process UV/H2O2. Water Res. 74, 143–154. https://doi.org/10.1016/j.watres.2014.12.039.

Bai, C., Colombo, P., 2018. Processing, properties and applications of highly porous geopolymers: a review. Ceram. Int. 44, 16103–16118. https://doi.org/10.1016/j.ceramint.2018.05.219.

Bai, C., Franchin, G., Elsayed, H., Conte, A., Colombo, P., 2016. High strength metakaolin-based geopolymer foams with variable macroporous structure. J. Eur. Ceram. Soc. 36, 4243–4249. https://doi.org/10.1016/j.jeurceramsoc.2016.06.045.

Bai, C., Franchin, G., Elsayed, H., Zaggia, A., Conte, L., Li, H., Colombo, P., 2017. High-porosity geopolymer foams with tailored porosity for thermal insulation and wastewater treatment. J. Mater. Res. 32, 3251–3259. https://doi.org/10.1557/jmr.2017.127.

Barona, J.F., Morales, D.F., González-Bahamón, L.F., Pulgarín, C., Benítez, L.N., 2015. Shift from heterogeneous to homogeneous catalysis during resorcinol degradation using the solar photo-Fenton process initiated at circumneutral pH. Appl. Catal. B Environ. 165, 620–627. https://doi.org/10.1016/j.apcatb.2014.10.053.

Bernal, S.A., Provis, J.L., 2014. Durability of alkali-activated materials: progress and perspectives. J. Am. Ceram. Soc. 97, 997–1008. https://doi.org/10.1111/jace.12831.

Bitenc, M., Horvat, B., Likozar, B., Dražić, G., Orel, Z.C., 2013. The impact of ZnO load, stability and morphology on the kinetics of the photocatalytic degradation of caffeine and resazurin. Appl. Catal. B Environ. 136–137, 202–209. https://doi.org/10.1016/j.apcatb.2013.02.016.

Charcosset, C., 2009. A review of membrane processes and renewable energies for desalination. Desalination 245, 214–231. https://doi.org/10.1016/j.desal.2008.06.020.

Cilla, M.S., Morelli, M.R., Colombo, P., 2014. Open cell geopolymer foams by a novel saponification/peroxide/gelcasting combined route. J. Eur. Ceram. Soc. 34, 3133–3137. https://doi.org/10.1016/j.jeurceramsoc.2014.04.001.

Clausi, M., Pinto, D., 2023. Valorisation of water potabilization sludges as precursors for alkali-activated binders: characterization and feasibility study. Materials 16. https://doi.org/10.3390/ma16051998.

Davidovits, J., 1991. Geopolymers. J. Therm. Anal. 37, 1633–1656. https://doi.org/10.1007/BF01912193.

Duxson, P., Provis, J.L., Lukey, G.C., Mallicoat, S.W., Kriven, W.M., Van Deventer, J.S.J., 2005. Understanding the relationship between geopolymer composition,

microstructure and mechanical properties. Colloids Surfaces A Physicochem. Eng. Asp. 269, 47–58. https://doi.org/10.1016/j.colsurfa.2005.06.060.
Duxson, P., Fernández-Jiménez, A., Provis, J.L., Lukey, G.C., Palomo, A., van Deventer, J. S.J., 2007. Geopolymer technology: the current state of the art. J. Mater. Sci. 42, 2917–2933. https://doi.org/10.1007/s10853-006-0637-z.
D'Accolti, L., De Cataldo, A., Montagna, F., Esposito Corcione, C., Maffezzoli, A., 2023. The role of 3D printing in the development of a catalytic system for the heterogeneous Fenton process. Polymers. https://doi.org/10.3390/polym15030580.
D'Elia, A., Clausi, M., Fernández-Jiménez, A., Palomo, A., Eramo, G., Laviano, R., Pinto, D., 2023. Alkali-activated binary binders with carbonate-rich illitic clay. Polymers 15. https://doi.org/10.3390/polym15020362.
El Alouani, M., Alehyen, S., El Achouri, M., Taibi, M., 2019. Preparation, characterization, and application of metakaolin-based geopolymer for removal of methylene blue from aqueous solution. J. Chem. 2019, 4212901 https://doi.org/10.1155/2019/4212901.
Ettahiri, Y., Bouargane, B., Fritah, K., Akhsassi, B., Pérez-Villarejo, L., Aziz, A., Bouna, L., Benlhachemi, A., Novais, R.M., 2023. A state-of-the-art review of recent advances in porous geopolymer: applications in adsorption of inorganic and organic contaminants in water. Construct. Build. Mater. 395, 132269 https://doi.org/10.1016/j.conbuildmat.2023.132269.
Falah, M., MacKenzie, K.J.D., Knibbe, R., Page, S.J., Hanna, J.V., 2016. New composites of nanoparticle Cu (I) oxide and titania in a novel inorganic polymer (geopolymer) matrix for destruction of dyes and hazardous organic pollutants. J. Hazard Mater. 318, 772–782. https://doi.org/10.1016/j.jhazmat.2016.06.016.
Ferella, F., 2018. Optimization of a plant for treatment of industrial waste solutions: experimental and process analysis. J. Environ. Chem. Eng. 6, 377–385. https://doi.org/10.1016/j.jece.2017.12.018.
Fusco, C., Casiello, M., Pisani, P., Monopoli, A., Fanelli, F., Oberhauser, W., Attrotto, R., Nacci, A., D'Accolti, L., 2022. Steel slag as low-cost catalyst for artificial photosynthesis to convert CO2 and water into hydrogen and methanol. Sci. Rep. 12, 11378 https://doi.org/10.1038/s41598-022-15554-3.
Gedam, N., Neti, N.R., 2014. Carbon attrition during continuous electrolysis in carbon bed based three-phase three-dimensional electrode reactor: treatment of recalcitrant chemical industry wastewater. J. Environ. Chem. Eng. 2, 1527–1532. https://doi.org/10.1016/j.jece.2014.06.025.
Gökçe, H.S., Tuyan, M., Nehdi, M.L., 2021. Alkali-activated and geopolymer materials developed using innovative manufacturing techniques: a critical review. Construct. Build. Mater. 303, 124483 https://doi.org/10.1016/j.conbuildmat.2021.124483.
Grosvenor, A.P., Kobe, B.A., Biesinger, M.C., McIntyre, N.S., 2004. Investigation of multiplet splitting of Fe 2p XPS spectra and bonding in iron compounds. Surf. Interface Anal. 36, 1564–1574. https://doi.org/10.1002/sia.1984.
Huang, J., Wang, M., Luo, S., Li, Z., Ge, Y., 2023. In situ preparation of highly graphitized N-doped biochar geopolymer composites for efficient catalytic degradation of tetracycline in water by H2O2. Environ. Res. 219, 115166 https://doi.org/10.1016/j.envres.2022.115166.
Hurt, C., Brandt, M., Priya, S.S., Bhatelia, T., Patel, J., Selvakannan, P.R., Bhargava, S., 2017. Combining additive manufacturing and catalysis: a review. Catal. Sci. Technol. 7, 3421–3439. https://doi.org/10.1039/C7CY00615B.
Kavitha, V., Palanivelu, K., 2004. The role of ferrous ion in Fenton and photo-Fenton processes for the degradation of phenol. Chemosphere 55, 1235–1243. https://doi.org/10.1016/j.chemosphere.2003.12.022.
Khalifa, A.Z., Cizer, Ö., Pontikes, Y., Heath, A., Patureau, P., Bernal, S.A., Marsh, A.T.M., 2020. Advances in alkali-activation of clay minerals. Cement Concr. Res. 132, 106050 https://doi.org/10.1016/j.cemconres.2020.106050.
Lancellotti, I., Catauro, M., Ponzoni, C., Bollino, F., Leonelli, C., 2013. Inorganic polymers from alkali activation of metakaolin: effect of setting and curing on structure. J. Solid State Chem. 200, 341–348. https://doi.org/10.1016/J.JSSC.2013.02.003.
Lee, W.K.W., Van Deventer, J.S.J., 2003. Use of Infrared Spectroscopy to Study Geopolymerization of Heterogeneous Amorphous Aluminosilicates. https://doi.org/10.1021/la026127e.
Legrini, O., Oliveros, E., Braun, A.M., 1993. Photochemical processes for water treatment. Chem. Rev. 93, 671–698. https://doi.org/10.1021/cr00018a003.
Li, C.J., Zhang, Y.J., Chen, H., He, P.Y., Meng, Q., 2022. Development of porous and reusable geopolymer adsorbents for dye wastewater treatment. J. Clean. Prod. 348, 131278 https://doi.org/10.1016/j.jclepro.2022.131278.
Liu, Y., Jin, W., Zhao, Y., Zhang, G., Zhang, W., 2017. Enhanced catalytic degradation of methylene blue by α-Fe2O3/graphene oxide via heterogeneous photo-Fenton reactions. Appl. Catal. B Environ. 206, 642–652. https://doi.org/10.1016/j.apcatb.2017.01.075.
Lofrano, G., Rizzo, L., Grassi, M., Belgiorno, V., 2009. Advanced oxidation of catechol: a comparison among photocatalysis, Fenton and photo-Fenton processes. Desalination 249, 878–883. https://doi.org/10.1016/j.desal.2009.02.068.
Lu, M.-C., Chang, Y.-F., Chen, I.-M., Huang, Y.-Y., 2005. Effect of chloride ions on the oxidation of aniline by Fenton's reagent. J. Environ. Manag. 75, 177–182. https://doi.org/10.1016/j.jenvman.2004.12.003.
Luhar, I., Luhar, S., Abdullah, M.M., Razak, R.A., Vizureanu, P., Sandu, A.V., Matasaru, P.-D., 2021. A state-of-the-art review on innovative geopolymer composites designed for water and wastewater treatment. Materials. https://doi.org/10.3390/ma14237456.
Luukkonen, T., von Gunten, U., 2022. Oxidation of organic micropollutant surrogate functional groups with peracetic acid activated by aqueous Co(II), Cu(II), or Ag(I) and geopolymer-supported Co(II). Water Res. 223, 118984 https://doi.org/10.1016/j.watres.2022.118984.
Luukkonen, T., Heponiemi, A., Runtti, H., Pesonen, J., Yliniemi, J., Lassi, U., 2019. Application of alkali-activated materials for water and wastewater treatment: a review. Rev. Environ. Sci. Bio/Technol. 18, 271–297. https://doi.org/10.1007/s11157-019-09494-0.
Medpelli, D., Seo, J.-M., Seo, D.-K., 2014. Geopolymer with hierarchically meso-/macroporous structures from reactive emulsion templating. J. Am. Ceram. Soc. 97, 70–73. https://doi.org/10.1111/jace.12724.
Medri, V., Papa, E., Landi, E., Maggetti, C., Pinelli, D., Frascari, D., 2022. Ammonium removal and recovery from municipal wastewater by ion exchange using a metakaolin K-based geopolymer. Water Res. 225, 119203 https://doi.org/10.1016/j.watres.2022.119203.
Metin, S., Çifçi, D.İ., 2023. Chemical industry wastewater treatment by coagulation combined with Fenton and photo-Fenton processes. J. Chem. Technol. Biotechnol. 98, 1158–1165. https://doi.org/10.1002/jctb.7321.
Mills, P., Sullivan, J.L., 1983. A study of the core level electrons in iron and its three oxides by means of X-ray photoelectron spectroscopy. J. Phys. D Appl. Phys. 16, 723. https://doi.org/10.1088/0022-3727/16/5/005.
Novais, R.M., Pullar, R.C., Labrincha, J.A., 2020. Geopolymer foams: an overview of recent advancements. Prog. Mater. Sci. 109, 100621 https://doi.org/10.1016/j.pmatsci.2019.100621.
O'Dowd, K., Pillai, S.C., 2020. Photo-Fenton disinfection at near neutral pH: process, parameter optimization and recent advances. J. Environ. Chem. Eng. 8, 104063 https://doi.org/10.1016/j.jece.2020.104063.
Pantone, V., Annese, C., Fusco, C., Fini, P., Nacci, A., Russo, A., D'Accolti, L., 2017. One-pot conversion of epoxidized soybean oil (ESO) into soy-based polyurethanes by MoCl2O2 catalysis. Molecules. https://doi.org/10.3390/molecules22020333.
Papa, E., Landi, E., Miccio, F., Medri, V., 2022. K2O-Metakaolin-Based geopolymer foams: production, porosity characterization and permeability test. Materials. https://doi.org/10.3390/ma15031008.
Pignatello, J.J., Oliveros, E., Mackay, A., 2006. Advanced oxidation processes for organic contaminant destruction based on the Fenton reaction and related chemistry. Crit. Rev. Environ. Sci. Technol. 36, 1–84. https://doi.org/10.1080/10643380500326564.
Provis, J.L., Van Deventer, J.S.J., 2009. 1 - introduction to geopolymers. In: Provis, John L., van Deventer, J.S.J.B.T.-G. (Eds.), Woodhead Publishing Series in Civil and Structural Engineering. Woodhead Publishing, pp. 1–11. https://doi.org/10.1533/9781845696382.1.
Reynoso, A., Zizzias, J., Sacchetto, J., Gambetta, C., Natera, J., Massad, W.A., 2021. Complete benzothiazole elimination by the solar photo-Fenton process in aqueous and β-cyclodextrin solutions. New J. Chem. 45, 20214–20218. https://doi.org/10.1039/D1NJ02483C.
ŞefikaKaya, Y., 2019. Evaluation of color and COD removal by Fenton and photo-fenton processes from industrial paper wastewater. Journal 9, 1539–1550.
Sgarlata, C., Formia, A., Siligardi, C., Ferrari, F., Leonelli, C., 2022. Mine Clay Washing Residues as a Source for Alkali-Activated Binders. Materials (Basel). https://doi.org/10.3390/ma15010083.
Shehata, N., Sayed, E.T., Abdelkareem, M.A., 2021. Recent progress in environmentally friendly geopolymers: a review. Sci. Total Environ. 762, 143166 https://doi.org/10.1016/J.SCITOTENV.2020.143166.
Shi, C., Qu, B., Provis, J.L., 2019. Recent progress in low-carbon binders. Cement Concr. Res. 122, 227–250. https://doi.org/10.1016/j.cemconres.2019.05.009.
Suhadolnik, L., Pohar, A., Likozar, B., Čeh, M., 2016. Mechanism and kinetics of phenol photocatalytic, electrocatalytic and photoelectrocatalytic degradation in a TiO2-nanotube fixed-bed microreactor. Chem. Eng. J. 303, 292–301. https://doi.org/10.1016/j.cej.2016.06.027.
Suhadolnik, L., Pohar, A., Novak, U., Likozar, B., Mihelič, A., Čeh, M., 2019. Continuous photocatalytic, electrocatalytic and photo-electrocatalytic degradation of a reactive textile dye for wastewater-treatment processes: batch, microreactor and scaled-up operation. J. Ind. Eng. Chem. 72, 178–188. https://doi.org/10.1016/j.jiec.2018.12.017.
Vitola, L., Bajare, D., Palomo, A., Fernandez-Jimenez, A., 2020. Low-calcium, porous, alkali-activated materials as novel pH stabilizers for water media. Minerals. https://doi.org/10.3390/min10110935.
Vorontsov, A.V., 2019. Advancing Fenton and photo-Fenton water treatment through the catalyst design. J. Hazard Mater. 372, 103–112. https://doi.org/10.1016/j.jhazmat.2018.04.033.
Wang, S., Zhang, Y., 2023. Zero valent iron-electro-Fenton-peroxymonosulfate (ZVI-E-Fenton-PMS) process for industrial wastewater treatment. RSC Adv. 13, 15063–15076. https://doi.org/10.1039/D2RA06653J.
Wang, N., Zheng, T., Zhang, G., Wang, P., 2016. A review on Fenton-like processes for organic wastewater treatment. J. Environ. Chem. Eng. 4, 762–787. https://doi.org/10.1016/j.jece.2015.12.016.
Wu, K., Xie, Y., Zhao, J., Hidaka, H., 1999. Photo-Fenton degradation of a dye under visible light irradiation. J. Mol. Catal. Chem. 144, 77–84. https://doi.org/10.1016/S1381-1169(98)00354-9.
Zhang, Y.J., Liu, L.C., Ni, L.L., Wang, B.L., 2013. A facile and low-cost synthesis of granulated blast furnace slag-based cementitious material coupled with Fe2O3 catalyst for treatment of dye wastewater. Appl. Catal. B Environ. 138–139, 9–16. https://doi.org/10.1016/j.apcatb.2013.02.025.
Zhang, J., Shi, C., Zhang, Z., Ou, Z., 2017. Durability of alkali-activated materials in aggressive environments: a review on recent studies. Construct. Build. Mater. 152, 598–613. https://doi.org/10.1016/j.conbuildmat.2017.07.027.
Zhang, Y.J., Han, Z.C., He, P.Y., Chen, H., 2020. Geopolymer-based catalysts for cost-effective environmental governance: a review based on source control and end-of-

pipe treatment. J. Clean. Prod. 263, 121556 https://doi.org/10.1016/j.jclepro.2020.121556.
Zheng, Y., Xie, W., Yuan, S., 2022. Hydroxylamine promoted Fe(III) reduction in H2O2/soil systems for phenol degradation. Environ. Sci. Pollut. Res. 29, 30285–30296. https://doi.org/10.1007/s11356-021-18345-x.
Zhu, Y., Ji, S., Liang, W., Li, C., Nie, Y., Dong, J., Shi, W., Ai, S., 2022. A low-cost and eco-friendly powder catalyst: iron and copper nanoparticles supported on biochar/geopolymer for activating potassium peroxymonosulfate to degrade naphthalene in water and soil. Chemosphere 303, 135185. https://doi.org/10.1016/j.chemosphere.2022.135185.